Chaos, Solitons and Fractals 155 (2022) 111724

Contents lists available at ScienceDirect

Chaos, Solitons and Fractals

Nonlinear Science, and Nonequilibrium and Complex Phenomena

journal homepage: www.elsevier.com/locate/chaos

Network modeling-based identification of the switching targets between pyroptosis and secondary pyroptosis

Ligang Zhu[a,1], Xiang Li[a,b,1,*], Fei Xu[a,c,1], Zhiyong Yin[a], Jun Jin[a], Zhilong Liu[a], Hong Qi[d], Jianwei Shuai[a,b,c,e,*]

[a] Department of Physics, and Fujian Provincial Key Lab for Soft Functional Materials Research, Xiamen University, Xiamen 361005, China
[b] State Key Laboratory of Cellular Stress Biology, Innovation Center for Cell Signaling Network, Xiamen University, Xiamen 361102, China
[c] Oujiang Laboratory (Zhejiang Lab for Regenerative Medicine, Vision and Brain Health), Wenzhou Institute, University of Chinese Academy of Sciences, Wenzhou, Zhejiang 325001, China
[d] Complex Systems Research Center, Shanxi University, Taiyuan 030006, China
[e] National Institute for Data Science in Health and Medicine, Xiamen University, Xiamen 361102, China

ARTICLE INFO

Article history:
Received 16 October 2021
Accepted 9 December 2021

Keywords:
Pyroptosis
Secondary pyroptosis
Complex network
Bifurcation analysis
Potential landscape
Systems biology
COVID-19

ABSTRACT

The newly identified cell death type, pyroptosis plays crucial roles in various diseases. Most recently, mounting evidence accumulates that pyroptotic signaling is highly correlated with coronavirus disease 2019 (COVID-19). Thus, understanding the induction of the pyroptotic signaling and dissecting the detail molecular control mechanisms are urgently needed. Based on recent experimental studies, a core regulatory model of the pyroptotic signaling is constructed to investigate the intricate crosstalk dynamics between the two cell death types, i.e., pyroptosis and secondary pyroptosis. The model well reproduces the experimental observations under different conditions. Sensitivity analysis determines that only the expression level of caspase-1 or GSDMD has the potential to individually change death modes. The decrease of caspase-1 or GSDMD level switches cell death from pyroptosis to secondary pyroptosis. Besides, eight biochemical reactions are identified that can efficiently switch death modes. While from the viewpoint of bifurcation analysis, the expression level of caspase-3 is further identified and twelve biochemical reactions are obtained. The coexistence of pyroptosis and secondary pyroptosis is predicted to be observed not only within the bistable range, but also within proper monostable range, presenting two potential different control mechanisms. Combined with the landscape theory, we further explore the stochastic dynamic and global stability of the pyroptotic system, accurately quantifying how each component mediates the individual occurrence probability of pyroptosis and secondary pyroptosis. Overall, this study sheds new light on the intricate crosstalk of the pyroptotic signaling and uncovers the regulatory mechanisms of various stable state transitions, providing potential clues to guide the development for prevention and treatment of pyroptosis-related diseases.

1. Introduction

Cell death plays important roles in homeostasis and diseases. Pyroptosis, one of the major types of cell death has been widely studied most recently [1]. Pyroptosis triggers a strong inflammatory response, leading to the pathology of various diseases, such as immune disease, metabolic disease, cardiovascular disease, Alzheimer's disease, and cancer [2–4]. Moreover, a recent clinical study shows that up to 63% of people infected with COVID-19 are highly correlated with pyroptotic death signaling [5]. Currently, many pyroptotic signaling inhibitors have exerted great function on COVID-19 treatment. The inhibitors, such as chloroquine and hydroxychloroquine, have been reported to effectively prevent the binding of SARS-CoV-2, which has been included in the treatment guidelines of COVID-19 [6]. Anakinra and disulfiram, which prevent the inflammatory storm induced by pyroptotic signaling, was recently used in COVID-19 treatment experiment [7]. Thus, understanding the regulatory mechanism of pyroptotic signaling is urgent for disease prevention and treatment.

Pyroptotic cell death is performed by the gasdermin family proteins, allowing the release of various damage/danger-associated molecular patterns (DAMPs), such as lactate dehydrogenase (LDH),

* Corresponding authors at: Department of Physics, and Fujian Provincial Key Lab for Soft Functional Materials Research, Xiamen University, Xiamen 361005, China.
E-mail addresses: xianglibp@xmu.edu.cn (X. Li), jianweishuai@xmu.edu.cn (J. Shuai).
[1] These authors contributed equally to this work.

https://doi.org/10.1016/j.chaos.2021.111724
0960-0779/

IL-1α, and IL-1β, from the lytic cells [3]. The released DAMPs in turn bind to pattern recognition receptors (PRRs), inducing subsequent inflammatory responses [8]. Pyroptosis is determined as a programmed cell death type since the executioner GSDMD was identified in 2015 [9–11]. GSDMD is the cleavage target for caspase-1. The cleaved GSDMD can form oligomeric pores on the cell membrane, promoting the release of inflammatory cytokine. The experiments found that GSDMD can also be activated by caspase-4/5 through non-canonical inflammatory signaling, while caspase-8 can directly cleave and activate GSDMD to induce pyroptosis [12–16]. Moreover, in 2017, Shao and Rogers teams successively identified that GSDME, which is also activated by the pyroptotic signaling, is the executioner of secondary pyroptosis [17–19]. Different from pyroptosis, the release of IL-1β is absent in secondary pyroptosis [20]. IL-1β is a key factor for triggering and amplifying the inflammatory response, causing cytokine storm and inducing various diseases [3,21].

In contrast to the various diseases triggered by pyroptosis, secondary pyroptosis releases fewer inflammatory cytokines, which can reduce the occurrence of severe immune diseases [20]. Experiments confirmed that GSDME can inhibit tumor growth by enhancing the anti-tumor function of cells [22], and thus secondary pyroptosis can act as a tumor suppressor for cancer treatment [23]. Besides, the GSDME-derived caspase-3 inhibitors to protect mice from acute hepatic failure have been developed [24]. Therefore, exploring the connectivity of pyroptosis and secondary pyroptosis and their potential switching mechanisms are urgently needed.

Great achievements have been made in the study of how cell fates are determined by the intricate pyroptotic signaling. High expression level of GSDMD causes a rapidly induction of pyroptosis [25]. While when GSDMD or caspase-1/11 is deficiency, activation of caspase-3 drives secondary pyroptosis in cells with a high expression of GSDME [18,26–28], emphasizing the crosstalk dynamics of caspases, GSDMD and GSDME in specifying cell fates [29]. Besides the experimental studies, network modeling is also a powerful approach to dissect the complicated regulatory mechanism of biological systems [30–33]. Bifurcation analysis has been successfully employed to quantitatively elucidate the tumor-suppressive mechanisms and cell-fate determination [34]. The biphasic roles of RIP1 in determining the distinct cell death outcomes have also been revealed recently [35]. To systematically explore the regulatory mechanisms of the newly identified death types, a core regulatory network model is constructed based on the most recently experimental data. Both the sensitivity analysis and bifurcation analysis are performed to address the underlying switching mechanisms between pyroptosis and secondary pyroptosis. Besides, the recently developed potential landscape theory [36–38] is further utilized to describe the stochastic dynamic and global stability of the intricate crosstalk, which accurately quantifies the occurrence probability of different death modes. Overall, this study makes a quantitative analysis of the pyroptotic signaling control mechanism, providing possible therapeutic strategies for intervening various death modes.

2. Results

2.1. Data-driven modeling of the crosstalk between pyroptosis and secondary pyroptosis

To investigate the pyroptotic signaling, a coarse-grained model is proposed based on our current understanding of the crosstalk between pyroptosis and secondary pyroptosis. Our simplified model comprises seven key constituents, i.e., caspase-1, caspase-8, caspase-9, caspase-3, tBid, GSDMD, and GSDME (Fig. 1A). Upon stimulation, the formation of inflammasome promotes the activation of caspase-1, which quickly cleaves and activates GSDMD, inducing the occurrence of pyroptosis [9]. The cleaved GSDMD also promotes the activation of caspase-1 [39], forming a positive feedback loop for the induction of pyroptosis. Caspase-1 can activate caspase-8 directly, which is restricted by the cleaved GSDMD [28]. In addition, caspase-1 can directly activate caspase-3 [40] with slow dynamics, or cleave tBid and then activate caspase-9 to cleave caspase-3 through the intrinsic apoptotic pathway [27]. The cleaved caspase-3 also activates caspase-8/9, providing an efficient positive feedback loop for caspase-3 activation [41].

Meanwhile, the inflammasome also recruits and activates caspase-8, which is inhibited by caspase-1 [42]. Recent studies indicated that the activated caspase-8 also cleaves GSDMD to cause pyroptosis [14–16]. It is widely reported that the activated caspase-8 directly cleaves caspase-3 through the extrinsic apoptotic pathway, or cleaves tBid to activate caspase-3 through the intrinsic apoptotic pathway [43]. Most recently, the caspase-3-cleaved GSDME that determines the occurrence of secondary pyroptosis has been identified [17,19]. Similar to tBid, GSDME can also promote the activation of caspase-9, forming a positive feedback loop to facilitate the induction of secondary pyroptosis [43]. Emerging evidence suggests that pyroptosis and secondary pyroptosis compete with each other. Secondary pyroptosis suppresses pyroptosis through inhibiting GSDMD by caspase-3, while pyroptosis can block secondary pyroptosis through strongly inhibiting the activation of tBid, caspase-8, and caspase-3 by GSDMD [28,29,44]. The detailed biological background description and a complete schematic diagram of the crosstalk (Figure S1) can be found in Supplemental Files.

Based on the schematic network shown in Fig. 1A, we constructed a corresponding model comprising these seven constituents. The death decision-making process of the intricate crosstalk can be described by seven coupled ordinary differential equations (ODEs) presented below:

$$\frac{d[Casp1]}{dt} = (C1tot - [Casp1])\left(\frac{k_{S\_1} * S^{n1}}{K_{S\_1}^{n1} + S^{n1}} + \frac{k_{GD\_1} * [GSDMD]^{n2}}{K_{GD\_1}^{n2} + [GSDMD]^{n2}}\right) - d_{C1} * [Casp1], \tag{1}$$

$$\frac{d[Casp8]}{dt} = (C8tot - [Casp8])\left(\frac{k_{S\_C8} * S^{n3}}{K_{S\_C8}^{n3} + S^{n3}} * \frac{J_{C1\_C8}^{n4}}{J_{C1\_C8}^{n4} + [Casp1]^{n4}} + \frac{k_{C3\_C8} * [Casp3]^{n5}}{K_{C3\_C8}^{n5} + [Casp3]^{n5}} + \frac{k_{C1\_C8} * [Casp1]^{n6}}{K_{C1\_C8}^{n6} + [Casp1]^{n6}} * \frac{K_{GD\_C8}^{n7}}{K_{GD\_C8}^{n7} + [GSDMD]^{n7}}\right) - d_{C8} * [Casp8] \tag{2}$$

$$\frac{d[Casp9]}{dt} = (C9tot - [Casp9])\left(\frac{k_{t\_C9} * [tBid]^{n8}}{K_{t\_C9}^{n8} + [tBid]^{n8}} + \frac{k_{GE\_C9} * [GSDME]^{n9}}{K_{GE\_C9}^{n9} + [GSDME]^{n9}} + \frac{k_{C3\_C9} * [Casp3]^{n10}}{K_{C3\_C9}^{n10} + [Casp3]^{n10}}\right) - d_{C9} * [Casp9], \tag{3}$$

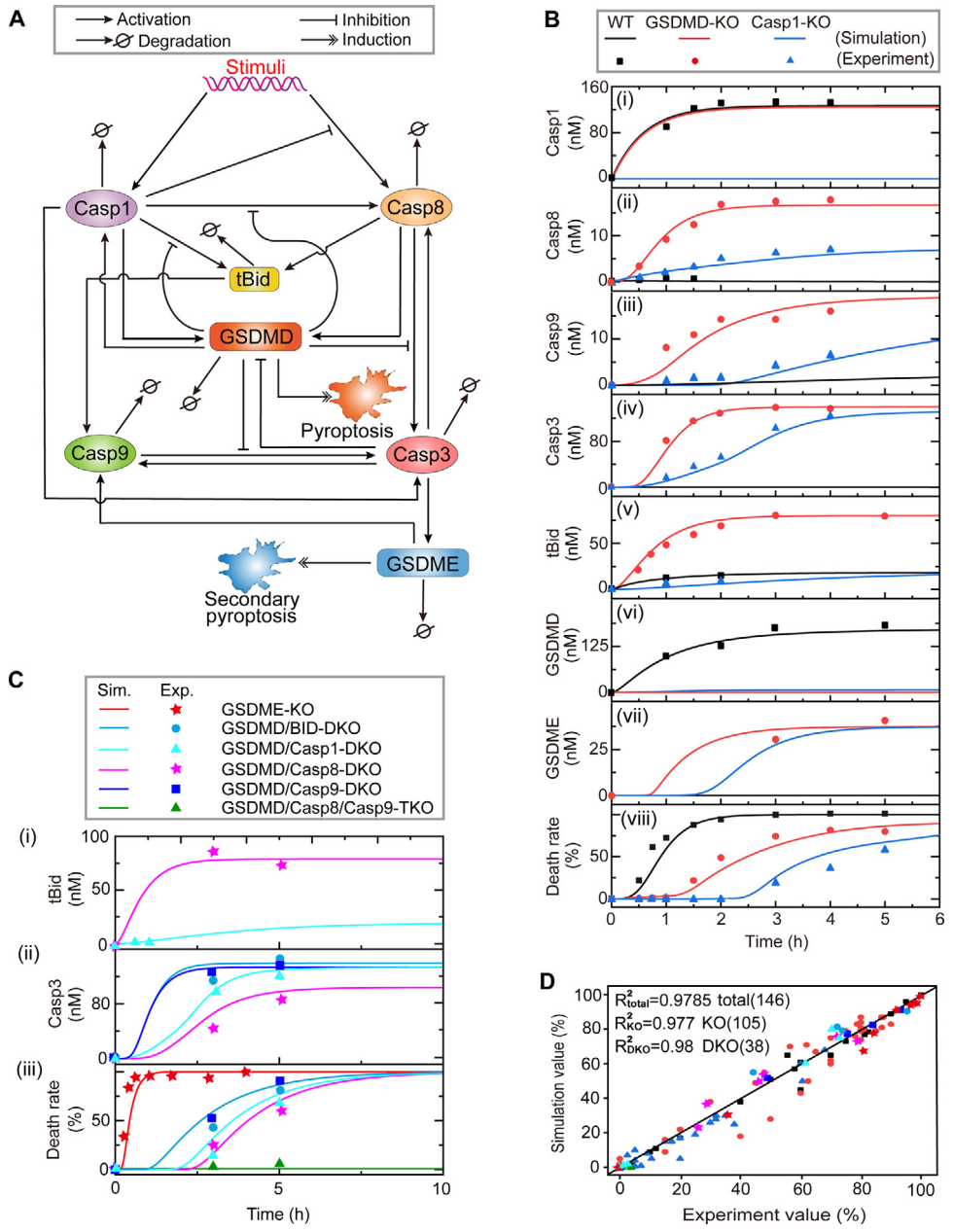

Fig. 1. Modeling the crosstalk between pyroptosis and secondary pyroptosis network. (A) The simplified regulatory network of pyroptosis and secondary pyroptosis signaling. (B) Comparison between experimental data (dots) and simulation results (lines) of the constituent time-course responses. The results of three different single constituent knockout conditions are colored by black (wild-type, WT), red (GSDMD knockout, GSDMD-KO) and blue (caspase-1 knockout, Casp1-KO). (C) Comparison between experimental data (dots) and simulation results (lines) in GSDME KO, GSDMD/BID DKO, GSDMD/Casp1 DKO, GSDMD/Casp8 DKO, GSDMD/Casp9 DKO, and GSDMD/Casp8/Casp9 TKO BMDMs. (D) Scatter diagram of experimental data versus simulation results. There are 27 comparison results for wild-type (WT), 78 comparison results for single knockout (KO), 30 comparison results for double knockout (DKO) and 3 comparison results for triple knockout (TKO) with a total of 138 comparison results. R^2 reflects the correlation strength between simulation results and experimental data.

$$\frac{d[Casp3]}{dt} = (C3tot - [Casp3])\left(\frac{k_{C8\_C3} * [Casp8]^{n11}}{K_{C8\_C3}^{n11} + [Casp8]^{n11}} * \frac{K_{GD\_C3}^{n12}}{K_{GD\_C3}^{n12} + [GSDMD]^{n12}} + \frac{k_{C9\_C3} * [Casp9]^{n13}}{K_{C9\_C3}^{n13} + [Casp9]^{n13}} * \frac{K_{GD\_C9}^{n14}}{K_{GD\_C9}^{n14} + [GSDMD]^{n14}} + \frac{k_{C1\_C3} * [Casp1]^{n15}}{K_{C1\_C3}^{n15} + [Casp1]^{n15}}\right) - d_{C3} * [Casp3], \quad (4)$$

$$\frac{d[tBid]}{dt} = (BIDtot - [tBid])\left(\frac{k_{C1\_t} * [Casp1]^{n16}}{K_{C1\_t}^{n16} + [Casp1]^{n16}} * \frac{K_{GD\_t}^{n17}}{K_{GD\_t}^{n17} + [GSDMD]^{n17}} + \frac{k_{C8\_t} * [Casp8]^{n18}}{K_{C8\_t}^{n18} + [Casp8]^{n18}}\right) - d_t * [tBid], \quad (5)$$

$$\frac{d[GSDMD]}{dt} = (GDtot - [GSDMD])\left(\frac{k_{C1\_GD} * [Casp1]^{n19}}{K_{C1\_GD}^{n19} + [Casp1]^{n19}} + \frac{k_{C8\_GD} * [Casp8]^{n20}}{K_{C8\_GD}^{n20} + [Casp8]^{n20}}\right) * \frac{K_{GD\_C3}^{n21}}{K_{GD\_C3}^{n21} + [Casp3]^{n21}} - d_{GD} * [GSDMD]. \quad (6)$$

$$\frac{d[GSDME]}{dt} = (GEtot - [GSDME]) * \frac{k_{C3\_} * [Casp3]^{n22}}{K_{C3\_}^{n22} + [Casp3]^{n22}} - d_{GE} * [GSDME]. \quad (7)$$

The dynamics of caspase-1 is described by Eq. (1), which mainly contains three terms. The first two terms respectively represent the activation of caspase-1 induced by stimuli and cleaved GSDMD. The last term describes the degradation/inactivation of caspase-1. Eq. (2) describes the dynamics of caspase-8, where the first term describes the activation of stimuli-induced caspase-8 activation, which is inhibited by caspase-1. The second term corresponds to the caspase-3-induced caspase-8 activation. While the last two terms represent the caspase-1-mediated caspase-8 activation that is blocked by GSDMD, and the degradation/inactivation of caspase-8, respectively. Eqs. (3) to (5) correspondingly describe the dynamics of caspase-3/9, and tBid. For the dynamics of the pyroptotic effector protein GSDMD in Eq. (6), the first two terms correspond to the processes of caspase-1/8-induced GSDMD activation that are suppressed by caspase-3, and the last term is for the degradation/inactivation of GSDMD. While for the secondary pyroptotic effector protein GSDME, Eq. (7) contains the terms of caspase-3-induced activation of GSDME and the degradation/inactivation of GSDME.

The dynamics of the cell population N is described by the following equation:

$$\frac{d[N]}{dt} = k_N * [N] - d_N * [N] * [N] - [N] * \left(\frac{k_{GD\_Np} * [GSDMD]^{n23}}{K_{GD\_Np}^{n23} + [GSDMD]^{n23}} + \frac{k_{GE\_Np} * [GSDME]^{n24}}{K_{GE\_Np}^{n24} + [GSDME]^{n24}} \right), \quad (8)$$

where the first two terms describe the basal cell proliferation and death [45]. The last two terms represent the population decrease induced by GSDMD-mediated pyroptosis and GSDME-mediated secondary pyroptosis. Cell death rate is defined by the ratio of the population of stimulus-induced cell death to the initial population of cell (steady state of non-stimulated cells), which is described by the formula of $(N_{init}\text{-}N)/N_{init}$, where Ninit is the initial population of cell.

The kinetic parameters in the model are mostly determined by a global optimization method that minimizes the deviation between simulation results and experimental data, and the rest parameters are estimated within a biologically plausible range based on previous literature. The experimental data are obtained from the study by Heilig et al. in bone marrow-derived macrophages (BMDMs) [27]. The deviation is characterized with the correlation coefficient, R-square, which is determined as the following functions:

$$R^2 = 1 - \frac{\sum_{i=1}^{n} (y_{exp}(t_i) - y_{sim}(t_i))^2}{\sum_{i=1}^{n} (y_{exp}(t_i) - \overline{y_{exp}})^2}, \quad (9)$$

where $y_{exp}(t_i)$ and $y_{sim}(t_i)$ are experimental data and simulation results of constituents at time t_i, respectively. The total amounts of the constituents are also estimated based on the experimental study. All the constituent descriptions and values are elaborated in Table S1. Detailed description of each parameter and their corresponding values can be found in Table S2.

We examine the reliability of the model through comparing with the experimental data under the conditions of wild-type (WT), caspase-1 knockout (KO), GSDMD KO, as well as the conditions of double constituents KO and triple constituents KO (Fig. 1B,C) in BMDMs. For the WT BMDMs (Fig. 1Bi, black line), caspase-1 is quickly activated after stimulation. Then GSDMD is activated to induce pyroptosis (Fig. 1Bvi and Bviii, black lines). While the other caspase-3/8/9, tBid, and GSDME are almost inactivated (Fig. 1Bi-Bvii, black lines) since the inhibition effects of GSDMD. For single caspase-1 KO or GSDMD KO BMDMs (red and blue lines in Fig. 1B), caspase-8 can be activated, leading to the activation of tBid, caspase-3/9, and the downstream GSDME. Both caspase-1 KO and GSDMD KO can respectively turn cells from pyroptosis to secondary pyroptosis, while the activation dynamics of caspase-3/8/9 and GSDME are significantly different. Compared with caspase-1 KO, GSDMD KO induces a rapid response of the constituents, resulting in a faster cell death pattern (Fig. 1B (viii)). The dynamics of the constituents double KO and triple KO cases given by our model are also quantitatively supported by the experimental observations (Fig. 1C) and the fitting results can be reflected clearly by the statistical chart shown in Fig. 1D. Overall, the excellent fitting between the simulation and experiment indicates that our model has high confidence for further clarifying the mechanisms of death mode switching between pyroptosis and secondary pyroptosis.

2.2. Sensitivity analysis reveals the switching mechanisms between pyroptosis and secondary pyroptosis

To determine whether and how the components mediate the death mode switching between pyroptosis and secondary pyroptosis, sensitivity analysis is conducted in this section. We first explore the effects of the expression level of the seven constituents on the death mode switching (Fig. 2A,B). The sensitivity of the downstream effector proteins, the cleaved GSDMD for pyroptosis, and the cleaved GSDME for secondary pyroptosis to the change of each constituent are investigated. We vary the level of each constituent individually in the range of 0.001–1000 nM to inquire the activation of GSDMD and GSDME. As the results shown, the increase of caspase-1 (C1tot) or GSDMD (GDtot) expression level enhances the GSDMD activation (Fig. 2A, left panel) and restrains the GSDME activation (Fig. 2B, left panel), presenting a death mode switching from secondary pyroptosis to pyroptosis. While the variation of the other five constituents (C8tot, C9tot, C3tot, BIDtot, and GEtot) barely affects cell death mode. The corresponding two-dimensional heat maps are presented in the right panels of Fig. 2A and B. These results are consistent with the experimental observations that GSDMD or caspase-1 is required for the switching between pyroptosis and secondary pyroptosis [18,20,27,28,46].

The pyroptotic crosstalk signaling totally includes 29 biochemical reactions, which are described by 45 kinetic parameters. We next discuss the key reactions in the crosstalk that can effectively switch the death mode. There are two kinds of parameters in the equations, i.e., the reaction rates and the Michaelis constants. Since the parameters of reaction rates and Michaelis constants have different biological ranges [47], we severally set their ranges within $10^{-7}\sim10^{-2}$ for the reaction rates and $10^{-3}\sim10^{3}$ for the Michaelis constants. The parameter sensitivity analysis suggests that only 4 reaction rates (Fig. 2C) and 6 Michaelis constants parameters (Fig. 2D) can effectively switch the death mode between pyroptosis and secondary pyroptosis. These parameters correspond to 8 biochemical reactions in the crosstalk, i.e., the activation of caspase-1 induced by stimuli (k_{S_C1} and K_{S_C1}), the activation of GSDMD induced by caspase-1 (k_{C1_GD} and K_{C1_GD}), the activation of caspase-3 induced by caspase-1 (k_{C1_C3}), the caspase-8-induced activation of caspase-3 that inhibited by GSDMD (K_{GD_C3}), the caspase-9-induced activation of caspase-3 that inhibited by GSDMD (K_{GD_C9}), the activation of GSDMD inhibited by caspase-3 (K_{C3_GD}), the activation of GSDME induced by Caspase-3 (K_{C3_GE}), and the degradation of GSDMD (d_{GD}). Therefore, sensitivity analysis suggests that only the expression levels of GSDMD and caspase-1, and above 8 biochemical reactions can effectively switch the death mode of the pyroptotic signaling.

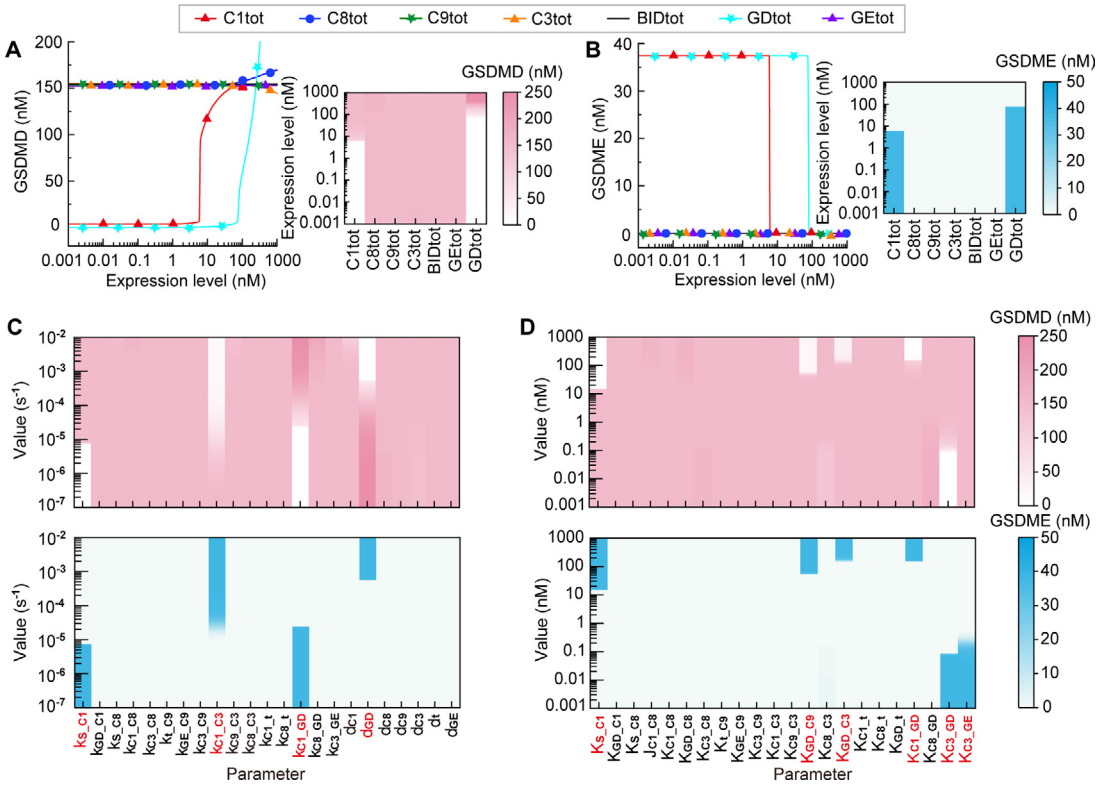

Fig. 2. Sensitivity analysis of constituent levels and reaction parameters. (A-B) The response curves and two-dimensional heat maps of GSDMD (A) and GSDME (B) to the level change from 0.001 nM to 1000 nM for the seven constituents. (C) The two-dimensional heat maps of GSDMD (upper panel) and GSDME (down panel) with the value change from 10^{-7} to 10^{-2} for the reaction rates. (D) The two-dimensional heat maps of GSDMD and GSDME with the value change from 0.001 to 1000 for the Michaelis constants.

2.3. Bifurcation analysis identifies the hidden components in switching death modes

Compared with sensitivity analysis, bifurcation analysis is a more comprehensive and widely used approach to study the state transition of various biological systems [48]. We therefore employ bifurcation analysis to evaluate the components that can switch death modes. Effects of the seven constituents expression levels on the death effector proteins, i.e., the cleaved GSDMD and GSDME are studied firstly. As shown in Fig. 3A, the caspase-1 expression level (C1tot) is conducted as the control parameter and the bifurcation diagram shows that the system presents monostability when the caspase-1 level is very low ($< \sim$1.5 nM) (blue region). The cleaved GSDMD is stable at a low level (upper panel), while the cleaved GSDME level is high (down panel). The death rate of an illustrative example (point A) is plotted in Fig. 3B, indicating that secondary pyroptosis occurs alone. The system exhibits bistability with the increase of caspase-1 expression level, which are enclosed by two saddle-node bifurcation points (SN1 and SN2) (green region). SN1 is the low threshold of the caspase-1 level ($\sim$1.5 nM) for GSDMD activation and GSDME inactivation, while SN2 is the high threshold ($\sim$14 nM) for GSDMD inactivation and GSDME activation. Within the bistable region, the stable state is sensitive to the initial condition of the activated caspase-3. For a certain caspase-1 expression level (e.g., C1tot = 10 nM), two stable states are given (point B and point C) (Fig. 3A) and a small perturbation of caspase-3 will drive the system to one of the two stable states. At the same level of caspase-1, when the initial activation level of the caspase-3 is 0 nM, GSDMD stays at a high level and GSDME activation is stabilized at a low level (Fig. 3A, point C), resulting in pyroptosis (Fig. 3B, point C). While a small initial activated caspase-3 (15 nM) can drive GSDME to a high steady state, and GSDMD converges to a low stable state (Fig. 3A, point B), inducing the concurrence of pyroptosis and secondary pyroptosis (Fig. 3B, point B). When the expression level of caspase-1 is high enough ($> \sim$14 nm), the system exhibits monostability and the cleaved GSDMD maintains at a high level, which gradually increases with the increase of caspase-1 (red region), while GSDME is stable at a quite low level, occurring pyroptosis only (Fig. 3B, point D).

The bifurcation diagrams of GSDMD level are similar to the results of caspase-1. The system presents monostability when GSDMD level is lower than $\sim$88 nM (Fig. 3C), inducing secondary pyroptosis alone (Fig. 3D, point 1), and exhibits bistability when GSDMD level ranging from 88 to 165 nM, in which cells will selectively execute the concurrence of pyroptosis and secondary pyroptosis (point 2) or pyroptosis alone (point 3) depending on the initial conditions. Pyroptosis alone will be exclusively induced (point 4) with higher level of GSDMD. Different from sensitivity analysis, bifurcation analysis reveals that the expression level of caspase-3 can also trigger bistability within the biologically plausible range (Fig. 3E). The cells execute only pyroptosis with low level of caspase-3 ($< \sim$250 nM), and selectively induce pyroptosis or secondary pyroptosis with higher level (Fig. 3F). Bifurcation diagrams of the other four constituent levels (caspase-8/9, GSDME, Bid) merely exhibit monostability, indicating that variations of the four constituents hardly affect the high steady states of GSDMD-induced pyroptosis (Fig. 3G). As a result, above bifurcation analysis suggests that only caspase-1, GSDMD, and caspase-3 expression levels among the seven constituents are capable to switch death modes between pyroptosis and secondary pyroptosis. Compared with sensitivity analysis, the switching role of caspase-3 is further identified by using bifurcation analysis.

Besides the constituents, whether and how the reactions mediate the cell death modes are discussed as well. Bifurcation dia-

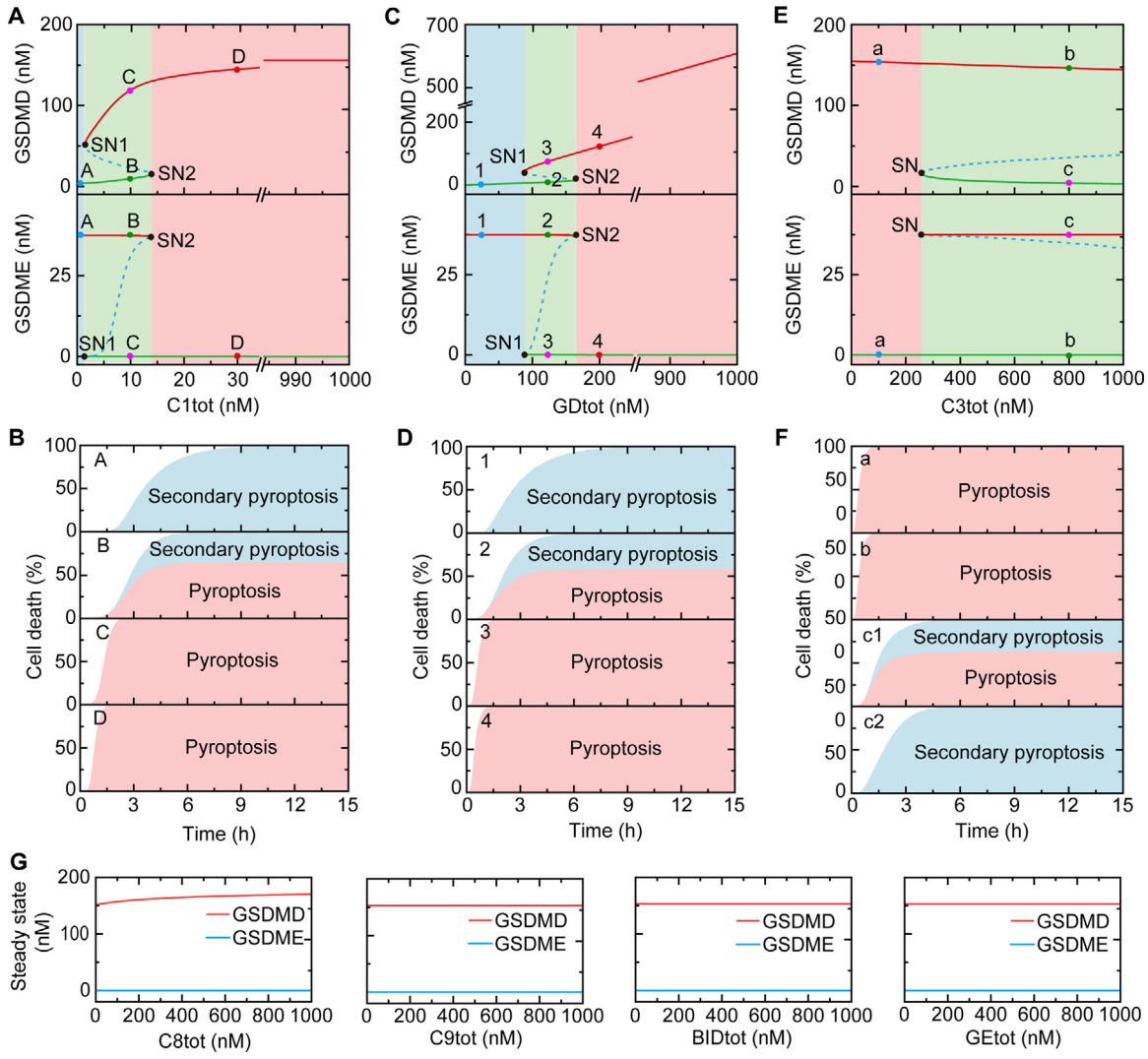

Fig. 3. Roles of constituent levels in death mode switching. (A) Bifurcation diagrams of GSDMD and GSDME as function of caspase-1 expression level (C1tot). Stable and unstable steady states are indicated by solid and dashed lines, respectively. (B) The contribution proportions of pyroptosis and secondary pyroptosis to cell death for points A–D in Fig. 3A, respectively. (C) Bifurcation diagrams of GSDMD and GSDME as function of GSDMD expression level (GDtot). (D) The contribution proportions of pyroptosis and secondary pyroptosis to cell death for points 1–4 in Fig. 3C, respectively. (E) Bifurcation diagrams of GSDMD and GSDME as function of caspase-3 expression level (C3tot). (F) The contribution proportions of pyroptosis and secondary pyroptosis to cell death for points a–c in Fig. 3E, respectively. (G) Bifurcation diagrams of GSDMD and GSDME as function of the expression level of caspase-8 expression level (C8tot), caspase-9 (C9tot), Bid (BIDtot), and GSDME (GEtot). In Fig. 3A, C, and E, the green areas are the bistability regions, while pink and blue areas correspond to monostability regions, respectively. In Fig. 3B, D and F, the pink and blue areas correspond to pyroptosis and secondary pyroptosis, respectively.

grams of activated GSDMD and GSDME as a function of the activation rate of caspase-1 induced by stimuli (parameter k_{S_C1}) are shown in Fig. 4A, presenting two different dynamical regions. A small value of parameter k_{S_C1} selectively induces the cells undergo pyroptosis or secondary pyroptosis depending on the initial conditions, while a large value of k_{S_C1} exclusively triggers pyroptosis (Fig. 4A,B). For the activation rate of GSDMD induced by caspase-1 (parameter k_{C1_GD}), the bifurcation diagrams present three different dynamical regions (Fig. 4C), which are similar to the results shown in Fig. 3C. A small value of parameter k_{C1_GD} triggers secondary pyroptosis alone, while the increase of k_{C1_GD} first converges the system to bistability with the concurrence of pyroptosis and secondary pyroptosis or pyroptosis alone, and then turns to the monostability region with the induction of pyroptosis. However, the system only presents monostability but can still switch cell death modes from pyroptosis to the concurrence of pyroptosis and secondary pyroptosis with the increase of the activation rate of caspase-3 induced by caspase-1 (parameter k_{C1_C3}).

There are totally 29 biochemical reactions that described by 45 parameters in the pyroptotic system. After scanning all the parameters, we find that 12 parameters, i.e., the activation rate/michaelis constant of caspase-1 induced by stimuli (k_{S_C1}/K_{S_C1}), the activation rate/michaelis constant of GSDMD induced by caspase-1 (k_{C1_GD}/K_{C1_GD}), the activation rate of caspase-3 activation induced by caspase-9 (k_{C9_C3}), michaelis constant for GSDMD inhibiting activation of caspase-3 induced by caspase-8/9 (K_{GD_C3}/K_{GD_C9}), the activation rate of caspase-3 activation induced by caspase-8 (k_{C8_C3}), michaelis constant for caspase-3 inhibiting the cleavage of GSDMD (K_{C3_GD}), and the degradation/inactivation rate of caspase-1/3 (d_{C1}/d_{C3}), and GSDMD (d_{GD}), can switch death modes through generating bistable state (Fig. S2). While for the rest parameters, the bifurcation diagrams only present monostability (Fig. S3). Among those parameters that exhibit monostability, two parameters, i.e., the activation rate of caspase-3 induced by caspase-1 (k_{C1_C3}) and the michaelis constant of GSDME cleaved by caspase-3 (K_{C3_GE}), can efficiently change the death modes between pyrop-

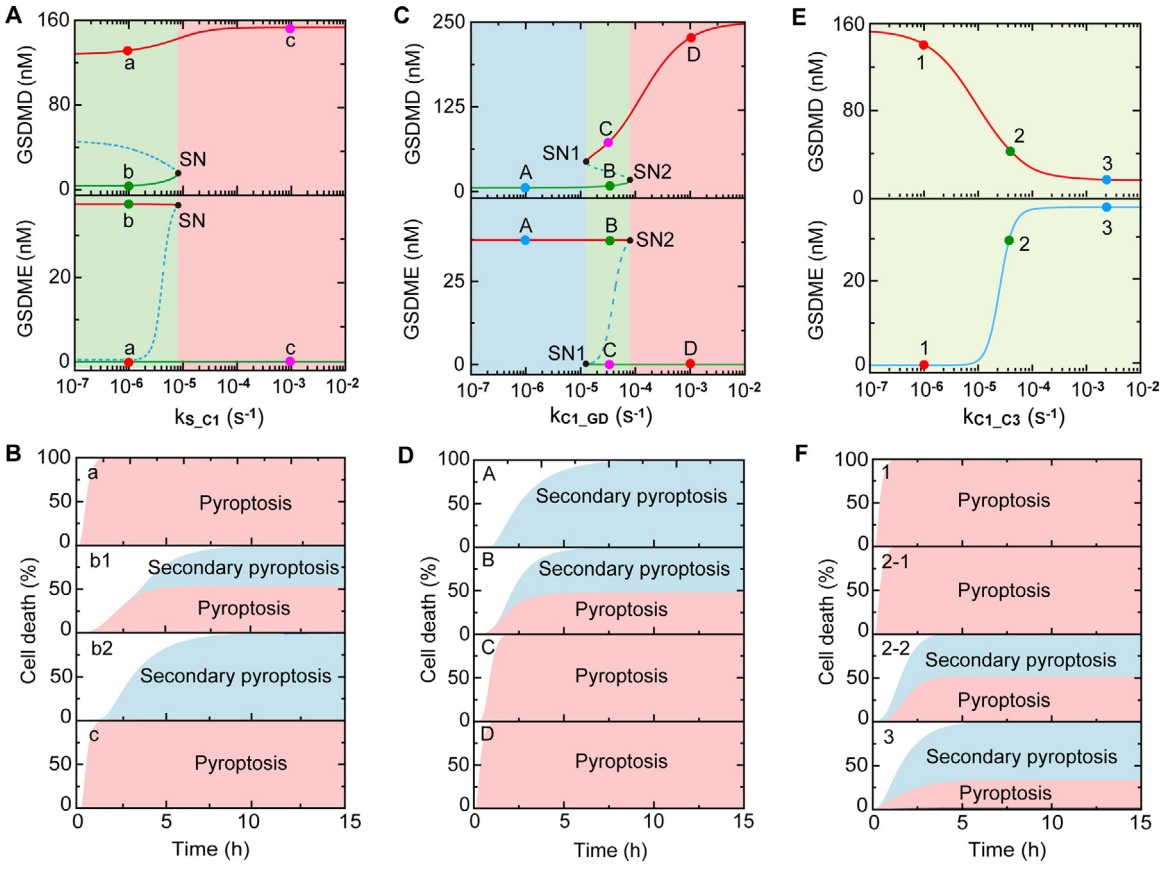

Fig. 4. Roles of reaction parameters in death modes switching. (A) Bifurcation diagrams of GSDMD and GSDME as function of the activation rate of caspase-1induced by stimuli (k_{S_C1}). Stable and unstable steady states are indicated by solid and dashed lines, respectively. (B) The contribution proportions of pyroptosis and secondary pyroptosis to cell death for points a-c in Fig. 4A, respectively. (C) Bifurcation diagrams of GSDMD and GSDME as function of the activation rate of GSDMD induced by caspase-1(k_{C1_GD}). (D) The contribution proportions of pyroptosis and secondary pyroptosis to cell death for points A-D in Fig. 4C, respectively. (E) Bifurcation diagrams of GSDMD and GSDME as function of the activation rate of caspase-3 induced by caspase-1 (k_{C1_C3}). (F) The contribution proportions of pyroptosis and secondary pyroptosis to cell death for points 1–3 in Fig. 4E, respectively.

tosis and secondary pyroptosis. Taken together, the 14 parameters mentioned above, which refer to 12 biochemical reactions in the intricate crosstalk signaling are determined. Compared with sensitivity analysis, one constituent (caspase-3), four hidden parameters that corresponds to 4 reactions, are further identified for modes switching by using the bifurcation analysis.

2.4. Potential landscape analysis dissects the global stability of the crosstalk

To systematically study the stochastic properties of the pyroptotic crosstalk switching mechanisms, a recently developed potential landscape theory that describes the global dynamic behavior of the system in phase space is further employed [36,37,49–52]. The dimensionless potential (U) and steady-state probability distribution (P) of the system is given by the Boltzmann relation, that is, U=-ln(P) [53,54]. We first investigate the effects of the expression level of the three identified constituents (caspase-1, GSDMD, and caspase-3) on the global stability of the system. The corresponding potential landscapes on the GSDMD-GSDME phase space are shown in Fig. 5. The yellow region represents higher potential or lower probability, and the blue region corresponds to lower potential or higher probability. As a result, the system exhibits monostable landscape when caspase-1 expression level is quite low (C1tot = 1 nM), implying that the system evolves into a unique state (secondary pyroptosis state) from any initial values (Fig. 5A). However, with a relative high caspase-1 level (C1tot = 2 nM), the landscape presents two basins of attraction, which characterizes two stable states (pyroptosis state and secondary pyroptosis state) (Fig. 5B). The system eventually evolves into one of the two basins from any initial conditions. The result shows that the secondary pyroptosis state is more stable than the pyroptosis state, indicating the high occurrence probability of secondary pyroptosis when caspase-1 expression level is low (Fig. 5B). As the caspase-1 level increases (C1tot = 14 nM), the secondary pyroptosis state becomes less stable while the pyroptosis state turns more stable (Fig. 5C), implying that the increase of caspase-1 promotes the induction of pyroptosis. When caspase-1 level is high enough (C1tot = 20 nM), the landscape changes from two coexisting stable states to the monostable pyroptosis state (Fig. 5D), suggesting that only pyroptosis occurs from any initial conditions. To quantify the landscape topography, we define the probability of cells evolve into the secondary pyroptosis state and pyroptosis state, which is associated with the height of the basin. As the results shown in Fig. 5E, too low (<∼ 1 nM) or too high (>∼15 nM) level of caspase-1 respectively induces the sole occurrence of secondary pyroptosis or pyroptosis. The occurrence probability of the secondary pyroptosis basin is decreased with the increase of caspase-1, while the probability of pyroptosis basin is increased. When the caspase-1 level is <∼9 nM, the probability of secondary pyroptosis is larger than pyroptosis. These results are consistent with the experimental observations that cells prefer secondary pyroptosis when caspase-1 expression level is low, but trend to pyroptosis with high caspase-1 level [18,20,46].

Similarly, the effects of the GSDMD and caspase-3 expression level on the landscape topography are discussed as well. As the

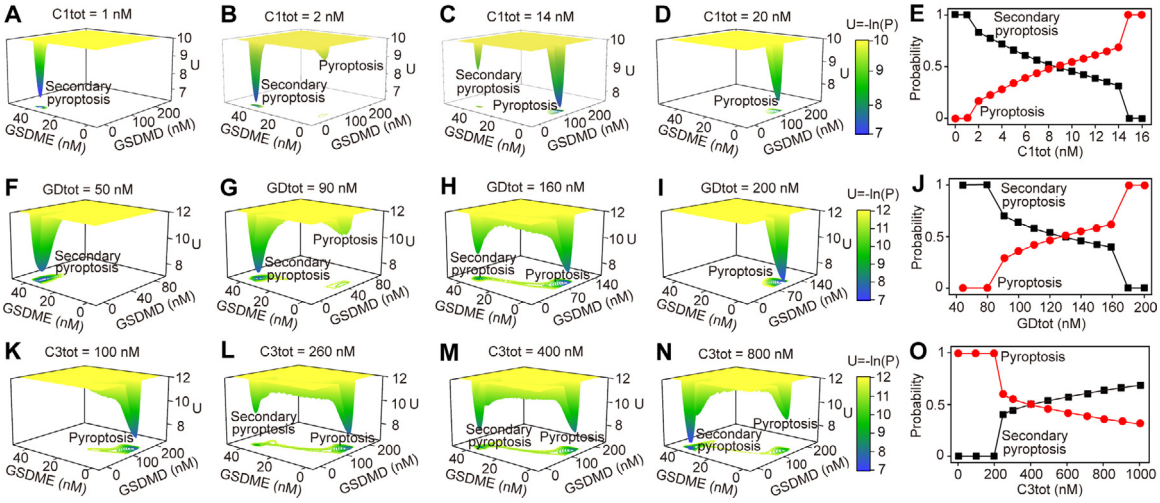

Fig. 5. Potential landscape changes as constituents level change. (A–D) Landscapes at different caspase-1 expression level (C1tot). (E) The occurrence probability of pyroptosis and secondary pyroptosis change as caspase-1 level changes. (F-I) Landscapes at different GSDMD expression level (GDtot). (J) The occurrence probability of pyroptosis and secondary pyroptosis change as GSDMD level changes. (K–N) Landscapes at different caspase-3 expression level (C3tot). (O) The occurrence probability of pyroptosis and secondary pyroptosis change as caspase-3 level changes.

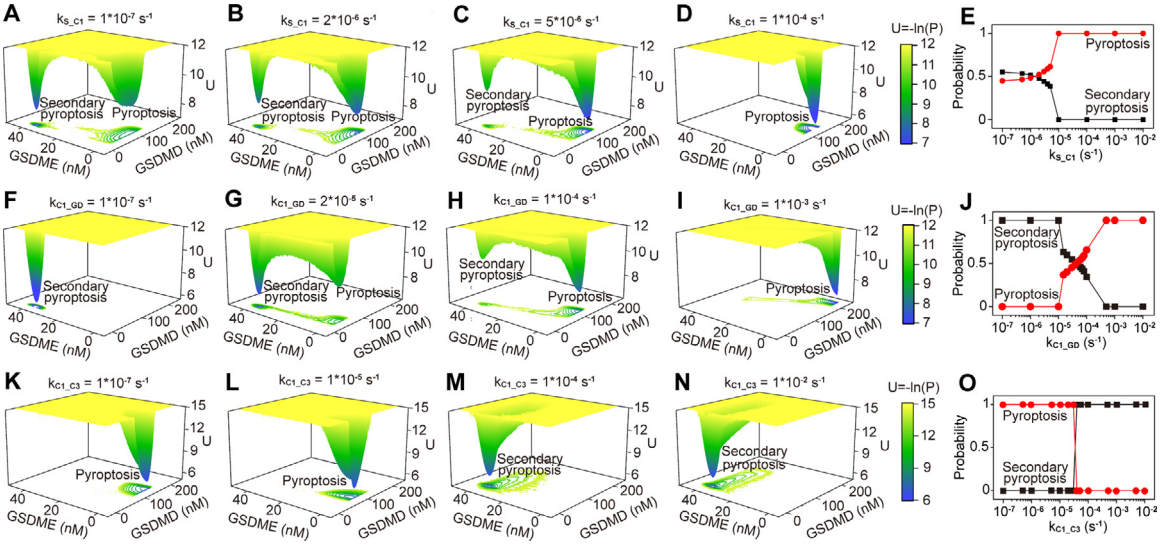

Fig. 6. Potential landscape changes as reaction rates change. (A–D) Landscapes at different values of k_{S_C1}. (E) The individual occurrence probabilities of pyroptosis and secondary pyroptosis change as k_{S_C1} changes. (F-I) Landscapes at different values of k_{C1_GD}. (J) The individual occurrence probabilities of pyroptosis and secondary pyroptosis change as k_{C1_GD} changes. (K–N) Landscapes at different values of k_{C1_C3}. (O) The occurrence probabilities of pyroptosis and secondary pyroptosis change as k_{C1_C3} changes.

results shown in Fig. 5F–I, increasing the GSDMD level increases the probability of cell death mode switching from secondary pyroptosis to pyroptosis. The occurrence probability of secondary pyroptosis is larger than pyroptosis when GSDMD level is lower than ~130 nM. (Fig. 5J) This is also supported by the experimental data [27,28,55,56]. However, increasing the caspase-3 level causes the decrease of the occurrence probability of secondary pyroptosis, but increases the probability of pyroptosis (Fig. 5K–N). The probability of pyroptosis is larger than secondary pyroptosis when caspase-3 level is lower than ~400 nM (Fig. 5O). Moreover, our result predicts that increasing the caspase-3 within the biologically plausible range can not switch the landscape to the monostable pyroptosis state, which needs to be further validated in experiments.

Besides the constituents, we also explore how the identified vital biochemical reactions (Fig. 4) determine the landscape topography of the system. For the activation rate of caspase-1 induced by stimuli (parameter k_{S_C1}), the landscapes present two basins of stable states when k_{S_C1} is small (Fig. 6A,B). The occurrence probability of pyroptosis becomes larger than the secondary pyroptosis when $k_{S\_C1} > \sim 1.5 \times 10^{-6}$ s^{-1}, and the landscape eventually evolves into the monostable pyroptosis state (Fig. 6D) when $k_{S\_C1} > \sim 10^{-5}$ s^{-1} (Fig. 6E). For the activation rate of GSDMD induced by caspase-1 (parameter k_{C1_GD}), the landscapes respectively exhibit monostable secondary pyroptosis state (Fig. 6F), two basins of stable state (Fig. 6G,H), and monostable pyroptosis state (Fig. 6I) with the increase of k_{C1_GD} (Fig. 6J). However, for the activation rate of caspase-3 induced by caspase-1 (parameter k_{C1_C3}), the system only presents monostable landscape (Fig. 6K–N). Increasing the k_{C1_C3} switches the monostable pyroptosis state to the secondary pyroptosis state, and the switching occurs when k_{C1_C3} equals to $\sim 2 \times 10^{-5}$ s^{-1} (Fig. 6L).

Therefore, potential landscape analysis provides a more physical description of the stochastic dynamic and global stability of the pyroptotic crosstalk. Compared with bifurcation analysis, a more accurate description of the transition dynamics of the system can be achieved through quantitatively calculating the individual occurrence probabilities of secondary pyroptosis and pyroptosis.

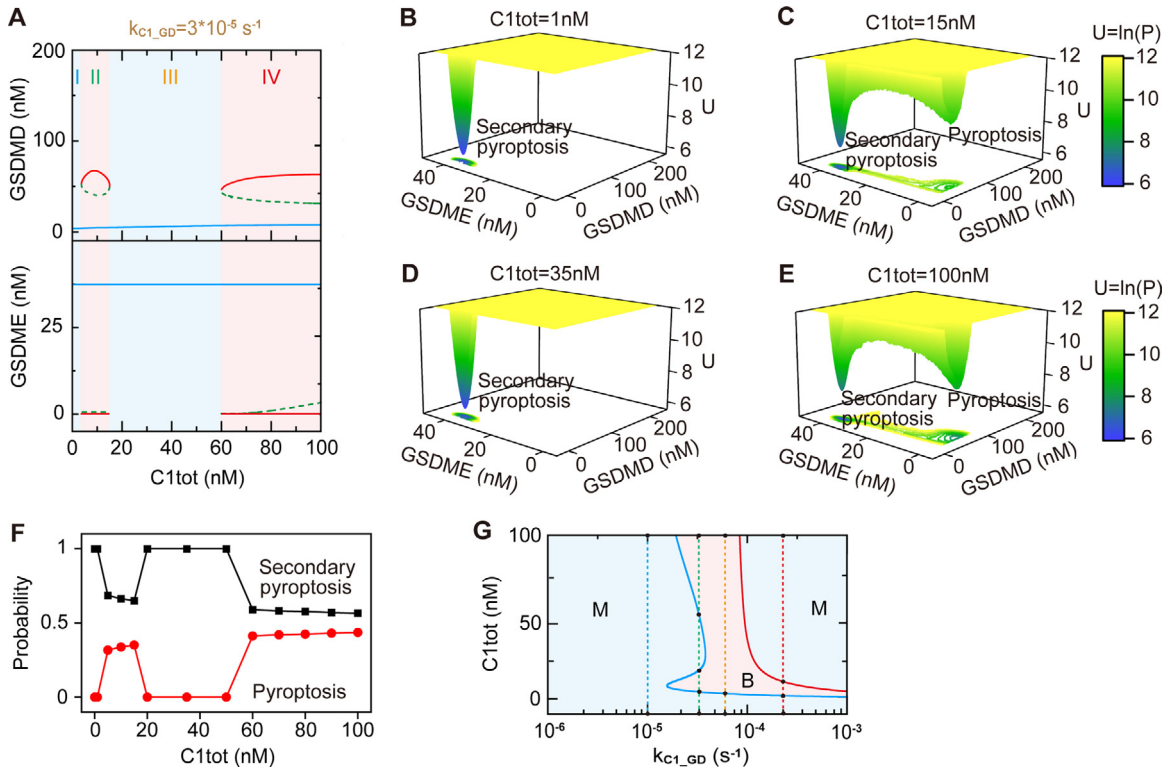

Fig. 7. Diverse states transition meditated by caspase-1 level and k_{C1_GD}. (A) Bifurcation diagrams of GSDMD and GSDME as function of caspase-1 level (C1tot) when $k_{C1\_GD}=3 \times 10^{-5}$ s^{-1}. As C1tot increases, the system presents monostability (region I), bistability (region II), monostability (region III), and bistability (region IV) in turn. (B–E) Landscapes at different expression levels of caspse-1 (C1tot) when $k_{C1\_GD}=3 \times 10^{-5}$ s^{-1}. (F) The occurrence probabilities of pyroptosis and secondary pyroptosis change as C1tot changes. (G) Phase diagram of the system stability on k_{C1_GD} with respect to C1tot. The blue area represents the monostable region (M) and pink area represents the bistable region (B).

2.5. Diverse stable states controlled by the constituent levels and reactions

The pyroptotic crosstalk could present a more diverse state transitions under certain conditions. As shown in Fig. 7A, the system first exhibits monostability, then bistability, and then monostability, finally bistability with the increasing expression level of caspase-1. Similarly, the influence of caspase-1 level on the potential landscape is shown in Fig. 7B–E, indicating that the system selectively presents monostable secondary pyroptosis landscape (C1tot = 1 nM and 35 nM), and the bistable secondary pyroptosis and pyroptosis landscape (C1tot = 15 nM and 100 nM). The individual occurrence probabilities of secondary pyroptosis and pyroptosis shown in Fig. 7F quantitatively appears the choice of death modes that depend on the initial conditions of caspase-1 level. We further conduct the two-parameter bifurcation diagram, which can display the synergistic modulation of multiple parameters on the diverse states transitions of the pyroptotic signaling. The phase diagram in the plane of multiple constituents or reactions provides a more holistic view of the states. The distribution of stable states with respect to different caspase-1 levels and the values of k_{C1_GD} is shown in Fig. 7G. With the increase of caspase-1 level, the states can be exclusively monostability (blue dashed line), four states switching (from monostability to bistability, to monostability, and to bistability) (green dashed line), two states switching (orange dashed line), and three states switching (red dashed line), depending on the value of k_{C1_GD}. A similar result of the state distribution is observed in the plane of k_{S_C1}-k_{C1_GD} (Figure S4), indicating the complicated role of k_{C1_GD} in mediating the diverse states transitions.

Accordingly, we next focus on the previously identified components that can switch death modes. Fig. 8A shows the distribution of stable states with respect to different caspase-1 and caspase-3 expression levels. With low level of caspase-3 expression ($<$ ~50 nM), monostable state for pyroptosis occurs alone with increasing caspase-1. A middle level of caspase-3 (~50 - ~140 nM) induces the states switching from bistable to monostable. While the change of states from monostability, to bistability, and finally to monostability are observed with high caspase-3 expression (~140 - ~240 nM). The bistable range becomes larger with the increasing caspase-3. Higher level of caspase-3 ($>$ ~240 nM) induces the transition from monostability to bistability. The diverse states distribution with respect to caspase-1/GSDMD and GSDMD/caspase-3 is shown in Fig. 8B and 8C. The phase diagrams with respect to the activation rate of GSDMD induced by caspase-1 (parameter k_{C1_GD}) and the three identified constituents are shown in Fig. 8D–F. All the other co-variation of parameters and constituents are explored and shown in Fig. S5. Moreover, the co-variation of two parameters that can switch death modes are also studied, presenting diverse states distributions (Fig. 8G–I). After scanning all the two-parameters bifurcation (Fig. S6), the four-state switching from monostability to bistability, to monostability, and to bistability can only be observed when k_{C1_GD} is considered (Fig. 8D, G, and H), suggesting the reaction of GSDMD activation by caspase-1 is dominant for various death mode determination.

3. Discussion

Extensive studies have focused on elucidating the molecular mechanisms of various types of cell death. While dissecting the emerging connectivity of different types of cell death and explore how these pathways synergistically work together to generate specific fate decision remain challenging [57,58]. Pyroptosis is related to various disease, while secondary pyroptosis appears harmless

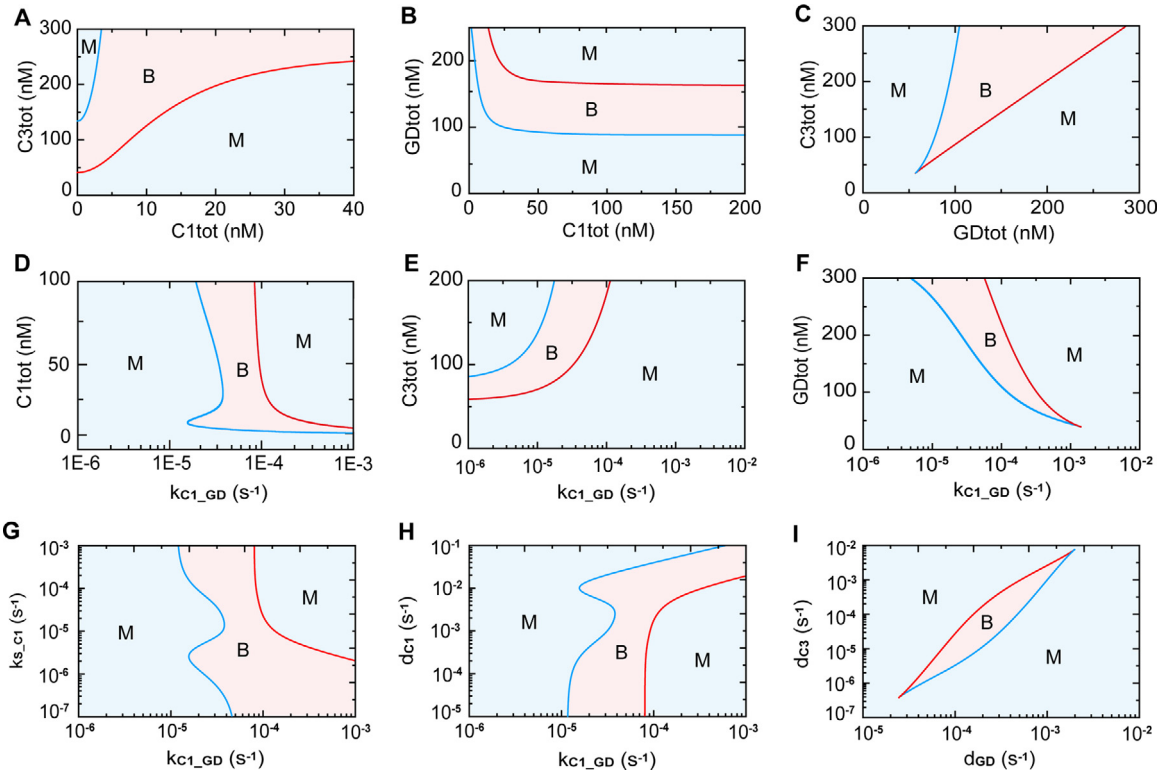

Fig. 8. Phase diagram of the system stability on the vital constituent levels and reactions. (A–C) Phase diagrams of the system stability on one of the three constituents level (C1tot, C3tot, and GDtot) with respect to another constituent. (D–F) Phase diagrams of the system stability on k_{C1_GD} (activation rate of GSDMD induced by caspase-1) with respect to the level of the three constituents, C1tot (D), C3tot (E) and GDtot (F). (G-H) Phase diagrams of the system stability on k_{C1_GD} (activation rate of GSDMD induced by caspase-1) with respect to the 2 key parameters, k_{S_C1} (activation rate of caspase-1 induced by stimuli) (G) and d_{C1} (inactivation/degradation rate of caspase-1) (H). (I) Phase diagram of the system stability on d_{GD} (inactivation/degradation rate of GSDMD) with respect to d_{C3} (inactivation/degradation rate of caspase-3).

and can inhibit tumor growth [23]. Thus, searching the potential strategies for efficiently switching death modes from pyroptosis to secondary pyroptosis is significant. Taken together with the most recently experimental observations, we constructed a coarse-grained model of the crosstalk between pyroptosis and secondary pyroptosis. We systematically study how each component and their combinations within the pyroptotic crosstalk determine the various death mode transitions. As a result, the deterministic components for mode switching are identified and shown in Fig. 9.

Sensitivity analysis indicates that the expression level of two constituents, i.e., GSDMD and caspase-1 can individually switch death modes between pyroptosis and secondary pyroptosis. Nevertheless, sensitivity analysis can only reveal the time-dynamical aspects. While with bifurcation analysis of stable state transition, we manifest the roles of three constituents, i.e., GSDMD, caspase-1, and caspase-3 in switching death modes. The switching roles of GSDMD and caspase-1 are consistent with previous experimental observations [18,20,27,28,46,55,56], while the predicted switching role of caspase-3 has not been experimentally reported. Besides, our results also suggest that varying the expression level of caspase-8/9, tBid, or GSDME could not efficiently switch the pyroptosis death mode. Thus, targeting on caspase-8/9, tBid, or GSDME for mode control might be invalid, which need to be further experimentally validated.

Compared with the eight biochemical reactions identified by sensitivity analysis, twelve reactions are determined by bifurcation analysis, which provides deeper insights into the regulatory mechanism of the crosstalk. The predicted multistability elucidates the mechanistic basis of various switches between pyroptosis and secondary pyroptosis. A more global view of multistability of the system is further clarified by using the phase diagram, reveal-

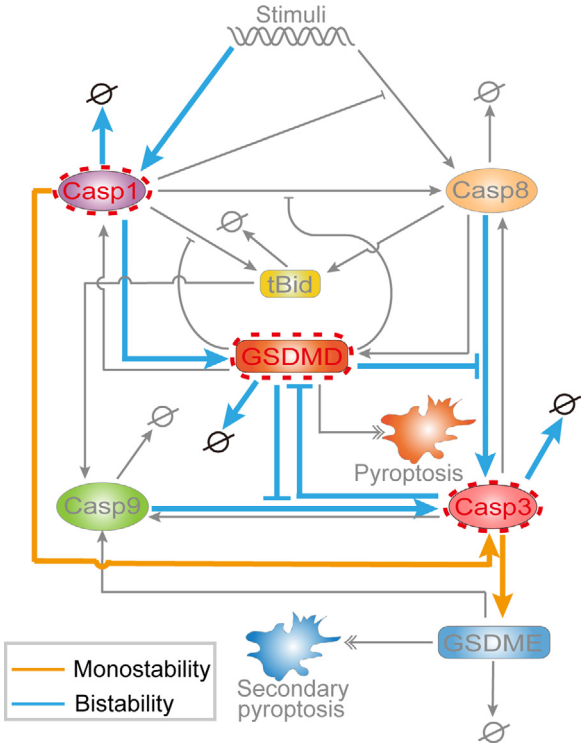

Fig. 9. Summary of the constituents and reactions that can switch cell death modes. The yellow and blue lines represent the reactions that can trigger monostability and bistability for switching death modes. Only changes in the expression level of caspase-1, caspase-3, or GSDMD can switch the cell death modes.

ing the possible molecular mechanisms in pathological cells. Although a "mutual inhibition" relationship between pyroptosis and secondary pyroptosis is generally assumed as many inhibition interaction among the crosstalk [27–29,44], the concurrence of pyroptosis and secondary pyroptosis is predicted to be observed under certain circumstances. Thus, there might be a "speed competition" between the two death modes. However, the coexistence of pyroptosis and secondary pyroptosis can also induce diseases, such as silicosis [59]. Thus, our proposed strategies for exclusively triggering secondary pyroptosis are especially important to guide the development for diseases prevention and treatment.

Mathematical modeling is a powerful approach and has successfully dissected many complex regulatory mechanisms of various cell death modes, such as apoptosis, necroptosis, and their crosstalk [35,48,60]. However, previous studies focused more on the deterministic dynamics [61–64]. Here, our study from the landscape viewpoint quantitatively provides the stochastic dynamics, the global nature, and the kinetic transitions of the pyroptotic signaling. This is the first landscape for the pyroptotic network, which involves the intricate crosstalk dynamics between pyroptosis and secondary pyroptosis. The landscape topography presents more dynamical properties of the signaling, such as the occurrence probability of secondary pyroptosis and pyroptosis that can be quantitatively calculated. Using this approach, we systematically study how the occurrence probabilities of the two death modes are determined by the key constituents and reactions, providing possible clues to design the effectiveness strategies in terms of different targets for death control.

Emerging evidences have suggested that the pyroptotic signaling plays important roles in COVID-19. The plasma levels of IL-1β and other inflammatory cytokines that are triggered by pyroptosis in patients infected with COVID-19 are much higher than those in healthy people [65]. Recent studies indicated that the spike (S) protein of SARS-CoV-2 binds to the ACE-2 receptor, which activates the NLRP3 inflammasome [7]. The caspase-1 in inflammasome further cleaves GSDMD, triggering the occurrence pyroptosis and severe immune response induced by IL-1β [66,67]. Besides, SARS-CoV-2 can also activate the AIM2 inflammasome to trigger pyroptosis and cytokine storm [7,68]. While the release of IL-1β is absent in secondary pyroptosis [20]. Therefore, targeting on potential components to switch the modes from pyroptosis to secondary pyroptosis could efficiently reduce the occurrence of cytokine storm in COVID-19.

At present, a number of pyroptotic signaling inhibitors have been proposed for COVID-19 clinical trial. Chloroquine and hydroxychloroquine, which can efficiently impair the binding of ACE-2 to SARS-CoV-2, and thus blocking the activation of inflammasome induced by SARS-CoV-2, have been partial applied in COVID-19 treatment [6]. Besides, a patient with COVID-19 was successfully treated with IL-1 receptor antagonist (anakinra) [69], which blocks the pro-inflammatory effect of IL-1 to trigger cytokine storm [70]. Bruton tyrosine kinase (BTK), which involved in inflammasome activation cascade, is also proposed to be a therapy target for COVID-19 [71]. In our study, we offer the theoretical guidance of potential targets for the treatment of COVID-19. As the summary shown in Fig. 9, we suggest that the three constituents, i.e., GSDMD, caspase-1, and caspase-3, and twelve biochemical reactions could be therapy target for COVID-19. Actually, for the proposed target of GSDMD, the GSDMD inhibitor, disulfiram, was recently applied in COVID-19 treatment experiment [7]. Moreover, the caspase-1 inhibitor, belnacasan (VX765) is also considered to have the therapeutic potential for COVID-19 [72]. However, for the proposed caspase-3 and the identified twelve reactions, there is no direct evidence right now. We hope these predictions can be further experimentally validated, or at least guide the development of potential strategies for COVID-19 treatment (Eqs. (4), (8), (9))

Data availability

The ODE model is developed and simulated with Python 3.8.2. Zipped mathematical code files of the model to generate the results in this study are available upon request from the corresponding author.

Declaration of Competing Interest

The authors declare that they have no known competing financial interests or personal relationships that could have appeared to influence the work reported in this paper.

CRediT authorship contribution statement

Ligang Zhu: Conceptualization, Formal analysis, Writing – original draft. **Xiang Li:** Conceptualization, Formal analysis, Funding acquisition, Writing – original draft. **Fei Xu:** Data curation, Formal analysis. **Zhiyong Yin:** Data curation, Validation. **Jun Jin:** Data curation, Validation. **Zhilong Liu:** Data curation, Validation. **Hong Qi:** Data curation, Validation. **Jianwei Shuai:** Funding acquisition, Writing – review & editing.

Acknowledgments

This work was supported by National Natural Science Foundation of China (Grants Nos. 12090052 and 11874310), the China Postdoctoral Science Foundation (Grant No. 2016M602071), and Shanxi Province Science Foundation for Youths (Grant No. 201901D211159).

Supplementary materials

Supplementary material associated with this article can be found, in the online version, at doi:10.1016/j.chaos.2021.111724.

References

[1] Galluzzi L, Vitale I, Aaronson SA, Abrams JM, Adam D, Agostinis P, et al. Molecular mechanisms of cell death: recommendations of the nomenclature committee on cell death 2018. Cell Death Differ 2018;25:486–541.
[2] Jia C, Chen H, Zhang J, Zhou K, Zhuge Y, Niu C, et al. Role of pyroptosis in cardiovascular diseases. Int Immunopharmacol 2019;67:311–18.
[3] Karki R, Sharma BR, Tuladhar S, Williams EP, Zalduondo L, Samir P, et al. Synergism of TNF-alpha and IFN-gamma triggers inflammatory cell death, tissue damage, and mortality in SARS-CoV-2 infection and cytokine shock syndromes. Cell. 2021;184:149–68 e17.
[4] Chaudhry H, Zhou J, Zhong Y, Ali MM, Mcguire F, Nagarkatti PS, et al. Role of cytokines as a double-edged sword in sepsis. In Vivo 2013;27:669–84.
[5] Huang C, Wang Y, Li X, Ren L, Zhao J, Hu Y, et al. Clinical features of patients infected with 2019 novel coronavirus in Wuhan, China. Lancet 2020;395:497–506.
[6] Qiu T, Liang S, Dabbous M, Wang Y, Han R, Toumi M. Chinese guidelines related to novel coronavirus pneumonia. Journal of Market Access & Health Policy 2020;8:1818446.
[7] Vora SM, Lieberman J, Wu H. Inflammasome activation at the crux of severe COVID-19. Nat Rev Immunol 2021;21:694–703.
[8] Bertheloot D, HMGB1 Latz E. IL-1alpha, IL-33 and S100 proteins: dual-function alarmins. Cell Mol Immunol 2017;14:43–64.
[9] He WT, Wan H, Hu L, Chen P, Wang X, Huang Z, et al. Gasdermin D is an executor of pyroptosis and required for interleukin-1beta secretion. Cell Res 2015;25:1285–98.
[10] Shi J, Zhao Y, Wang K, Shi X, Wang Y, Huang H, et al. Cleavage of GSDMD by inflammatory caspases determines pyroptotic cell death. Nature 2015;526:660–5.
[11] Liu X, Zhang Z, Ruan J, Pan Y, Magupalli VG, Wu H, et al. Inflammasome-activated gasdermin D causes pyroptosis by forming membrane pores. Nature 2016;535:153–8.
[12] Aglietti RA, Estevez A, Gupta A, Ramirez MG, Liu PS, Kayagaki N, et al. GsdmD p30 elicited by caspase-11 during pyroptosis forms pores in membranes. Proc Natl Acad Sci U S A 2016;113:7858–63.
[13] Kayagaki N, Stowe IB, Lee BL, O'Rourke K, Anderson K, Warming S, et al. Caspase-11 cleaves gasdermin D for non-canonical inflammasome signalling. Nature 2015;526:666–71.

[14] Orning P, Weng D, Starheim K, Ratner D, Best Z, Lee B, et al. Pathogen blockade of TAK1 triggers caspase-8-dependent cleavage of gasdermin D and cell death. Science 2018;362:1064–9.
[15] Sarhan J, Liu BC, Muendlein HI, Li P, Nilson R, Tang AY, et al. Caspase-8 induces cleavage of gasdermin D to elicit pyroptosis during yersinia infection. Proc Natl Acad Sci U S A 2018;115:E10888–E10E97.
[16] Gram AM, Booty LM, Bryant CE. Chopping GSDMD: caspase-8 has joined the team of pyroptosis-mediating caspases. EMBO J 2019;38:e102065.
[17] Rogers C, Fernandes-Alnemri T, Mayes L, Alnemri D, Cingolani G, Alnemri ES. Cleavage of DFNA5 by caspase-3 during apoptosis mediates progression to secondary necrotic/pyroptotic cell death. Nat Commun 2017;8:14128.
[18] Schneider KS, Gross CJ, Dreier RF, Saller BS, Mishra R, Gorka O, et al. The inflammasome drives GSDMD-independent secondary pyroptosis and IL-1 release in the absence of caspase-1 protease activity. Cell Rep 2017;21:3846–59.
[19] Wang Y, Gao W, Shi X, Ding J, Liu W, He H, et al. Chemotherapy drugs induce pyroptosis through caspase-3 cleavage of a gasdermin. Nature 2017;547:99–103.
[20] Aizawa E, Karasawa T, Watanabe S, Komada T, Kimura H, Kamata R, et al. GSDME-dependent incomplete pyroptosis permits selective IL-1α release under caspase-1 inhibition. iScience 2020;23:101070.
[21] Ferreira AC, Soares VC, de Azevedo-Quintanilha IG, Dias S, Fintelman-Rodrigues N, Sacramento CQ, et al. SARS-CoV-2 engages inflammasome and pyroptosis in human primary monocytes. Cell Death Discov 2021;7:43.
[22] Zhang Z, Zhang Y, Xia S, Kong Q, Li S, Liu X, et al. Gasdermin E suppresses tumour growth by activating anti-tumour immunity. Nature 2020;579:415–20.
[23] Wang L, Qin X, Liang J, Ge P. Induction of pyroptosis: a promising strategy for cancer treatment. Front Oncol 2021;11:635774.
[24] Xu WF, Zhang Q, Ding CJ, Sun HY, Che Y, Huang H, et al. Gasdermin E-derived caspase-3 inhibitors effectively protect mice from acute hepatic failure. Acta Pharmacol Sin 2021;42:68–76.
[25] Liu Z, Wang C, Yang J, Chen Y, Zhou B, Abbott DW, et al. Caspase-1 engages full-length gasdermin d through two distinct interfaces that mediate caspase recruitment and substrate cleavage. Immunity 2020;53:106–14 e5.
[26] de Vasconcelos NM, Van Opdenbosch N, Van Gorp H, Martin-Perez R, Zecchin A, Vandenabeele P, et al. An apoptotic caspase network safeguards cell death induction in pyroptotic macrophages. Cell Rep 2020;32:107959.
[27] Heilig R, Dilucca M, Boucher D, Chen KW, Hancz D, Demarco B, et al. Caspase-1 cleaves Bid to release mitochondrial SMAC and drive secondary necrosis in the absence of GSDMD. Life Sci Alliance 2020;3:e202000735.
[28] Tsuchiya K, Nakajima S, Hosojima S, Thi Nguyen D, Hattori T, Manh Le T, et al. Caspase-1 initiates apoptosis in the absence of gasdermin D. Nat Commun 2019;10:2091.
[29] Taabazuing CY, Okondo MC, Bachovchin DA. Pyroptosis and apoptosis pathways engage in bidirectional crosstalk in monocytes and macrophages. Cell Chem Biol 2017;24:507–14 e4.
[30] Liu W, Li X, Qi H, Wu Y, Qu J, Yin Z, et al. Biphasic regulation of transcriptional surge generated by the gene feedback loop in a two-component system. Bioinformatics 2021;37:2682–90.
[31] Li X, Zhong CQ, Yin Z, Qi H, Xu F, He Q, et al. Data-driven modeling identifies TIRAP-independent MyD88 activation complex and myddosome assembly strategy in LPS/TLR4 signaling. Int J Mol Sci 2020;21.
[32] Rocha Filho TM, Moret MA, Chow CC, Phillips JC, Cordeiro AJA, Scorza FA, et al. A data-driven model for COVID-19 pandemic - evolution of the attack rate and prognosis for Brazil. Chaos Solitons Fractals 2021;152:111359.
[33] Ghanbari B. On forecasting the spread of the COVID-19 in Iran: the second wave. Chaos Solitons Fractals 2020;140:110176.
[34] Tian X, Huang B, Zhang XP, Lu M, Liu F, Onuchic JN, et al. Modeling the response of a tumor-suppressive network to mitogenic and oncogenic signals. Proc Natl Acad Sci U S A 2017;114:5337–42.
[35] Li X, Zhong CQ, Wu R, Xu X, Yang ZH, Cai S, et al. RIP1-dependent linear and nonlinear recruitments of caspase-8 and RIP3 respectively to necrosome specify distinct cell death outcomes. Protein Cell 2021;12:858–76.
[36] Kang X, Li C. A dimension reduction approach for energy landscape: identifying intermediate states in metabolism-EMT network. Adv Sci 2021;8:2003133 (Weinh).
[37] Shu J, Wu C, Wu Y, Li Z, Shao S, Zhao W, et al. Induction of pluripotency in mouse somatic cells with lineage specifiers. Cell 2013;153:963–75.
[38] Li X, Jin J, Zhang X, Xu F, Zhong J, Yin Z, et al. Quantifying the optimal strategy of population control of quorum sensing network in escherichia coli. NPJ Syst Biol Appl 2021;7:35.
[39] Ruhl S, Broz P. Caspase-11 activates a canonical NLRP3 inflammasome by promoting K(+) efflux. Eur J Immunol 2015;45:2927–36.
[40] Sagulenko V, Vitak N, Vajjhala PR, Vince JE, Stacey KJ. Caspase-1 Is an apical caspase leading to caspase-3 cleavage in the AIM2 inflammasome response, independent of caspase-8. J Mol Biol 2018;430:238–47.
[41] Cheng X, Ferrell JE. Apoptosis propagates through the cytoplasm as trigger waves. Science 2018;361:607–12.
[42] Lee BL, Mirrashidi KM, Stowe IB, Kummerfeld SK, Watanabe C, Haley B, et al. ASC- and caspase-8-dependent apoptotic pathway diverges from the NLRC4 inflammasome in macrophages. Sci Rep 2018;8:3788.
[43] Rogers C, Erkes DA, Nardone A, Aplin AE, Fernandes-Alnemri T, Alnemri ES. Gasdermin pores permeabilize mitochondria to augment caspase-3 activation during apoptosis and inflammasome activation. Nat Commun 2019;10:1689.
[44] Chen KW, Demarco B, Broz P. Beyond inflammasomes: emerging function of gasdermins during apoptosis and NETosis. EMBO J 2020;39:e103397.
[45] Charlebois DA, Balazsi G. Modeling cell population dynamics. In Silico Biol 2019;13:21–39.
[46] McKenzie BA, Mamik MK, Saito LB, Boghozian R, Monaco MC, Major EO, et al. Caspase-1 inhibition prevents glial inflammasome activation and pyroptosis in models of multiple sclerosis. Proc Natl Acad Sci U S A 2018;115:E6065–74.
[47] Albeck JG, Burke JM, Spencer SL, Lauffenburger DA, Sorger PK. Modeling a snap-action, variable-delay switch controlling extrinsic cell death. PLoS Biol 2008;6:2831–52.
[48] Qi H, Li X, Jin Z, Simmen T, Shuai J. The oscillation amplitude, not the frequency of cytosolic calcium, regulates apoptosis induction. iScience. 2020;23:101671.
[49] Li C, Wang J. Landscape and flux reveal a new global view and physical quantification of mammalian cell cycle. Proc Natl Acad Sci U S A 2014;111:14130–5.
[50] Ye Y, Kang X, Bailey J, Li C, Hong T. An enriched network motif family regulates multistep cell fate transitions with restricted reversibility. PLoS Comput Biol 2019;15:e1006855.
[51] Qiu K, Gao KF, Yang LJ, Zhang ZK, Wang R, Ma HS, et al. A kinetic model of multiple phenotypic states for breast cancer cells. Sci Rep 2017;7:9890.
[52] He P, Qiu K, Jia Y. Modeling of mesenchymal hybrid epithelial state and phenotypic transitions in EMT and MET processes of cancer cells. Sci Rep 2018;8:14323.
[53] Wang J, Li C, Wang E. Potential and flux landscapes quantify the stability and robustness of budding yeast cell cycle network. Proc Natl Acad Sci U S A 2010;107:8195–200.
[54] Wang J, Zhang K, Xu L, Wang E. Quantifying the Waddington landscape and biological paths for development and differentiation. Proc Natl Acad Sci U S A 2011;108:8257–62.
[55] Humphries F, Shmuel-Galia L, Ketelut-Carneiro N, Li S, Wang B, Nemmara VV, et al. Succination inactivates gasdermin D and blocks pyroptosis. Science 2020;369:1633–7.
[56] Kayagaki N, Lee BL, Stowe IB, Kornfeld OS, O'Rourke K, Mirrashidi KM, et al. IRF2 transcriptionally induces GSDMD expression for pyroptosis. Sci Signal 2019:12.
[57] Newton K, Wickliffe KE, Maltzman A, Dugger DL, Reja R, Zhang Y, et al. Activity of caspase-8 determines plasticity between cell death pathways. Nature 2019;575:679–82.
[58] Bedoui S, Herold MJ, Strasser A. Emerging connectivity of programmed cell death pathways and its physiological implications. Nat Rev Mol Cell Biol 2020;21:678–95.
[59] Mayeux JM, Escalante GM, Christy JM, Pawar RD, Kono DH, Pollard KM. Silicosis and silica-induced autoimmunity in the diversity outbred mouse. Front Immunol. 2018;9:874.
[60] Xu F, Yin Z, Zhu L, Jin J, He Q, Li X, et al. Oscillations governed by the incoherent dynamics in necroptotic signaling. Front Phys 2021;9:482.
[61] Ndairou F, Area I, Nieto JJ, Torres DFM. Mathematical modeling of COVID-19 transmission dynamics with a case study of Wuhan. Chaos Solitons Fractals 2020;135:109846.
[62] Malik YS, Obli Rajendran V, Ma I, Pande T, Ravichandran K, Jaganathasamy N, et al. Responses to COVID-19 in South Asian Association for Regional Cooperation (SAARC) countries in 2020, a data analysis during a world of crises. Chaos Solitons Fractals 2021;152:111311.
[63] Wu Y, Wang Q, Qu J, Liu W, Gao X, Li X, et al. Different response modes and cooperation modulations of blue-light receptors in photomorphogenesis. Plant Cell Environ 2021;44:1802–15.
[64] Li X, Chen Y, Qi H, Liu L, Shuai J. Synonymous mutations in oncogenesis and apoptosis versus survival unveiled by network modeling. Oncotarget 2016;7:34599–616.
[65] Huang Q, Wu X, Zheng X, Luo S, Xu S, Weng J. Targeting inflammation and cytokine storm in COVID-19. Pharmacol Res 2020;159:105051.
[66] Junqueira C, Crespo A, Ranjbar S, Ingber J, Parry B, Ravid S, et al. SARS-CoV-2 infects blood monocytes to activate NLRP3 and AIM2 inflammasomes, pyroptosis and cytokine release. medRxiv 2021 2021.03.06.21252796.
[67] Ma H, Zhu Z, Lin H, Wang S, Zhang P, Li Y, et al. Pyroptosis of syncytia formed by fusion of SARS-CoV-2 spike and ACE2-expressing cells. Cell Discov 2021;7:73.
[68] Nowill AE, de Campos-Lima PO. Immune response resetting as a novel strategy to overcome SARS-CoV-2-induced cytokine storm. J Immunol 2020;205:2566–75.
[69] Filocamo G, Mangioni D, Tagliabue P, Aliberti S, Costantino G, Minoia F, et al. Use of anakinra in severe COVID-19: a case report. Int J Infect Dis 2020;96:607–9.
[70] Huet T, Beaussier H, Voisin O, Jouveshomme S, Dauriat G, Lazareth I, et al. Anakinra for severe forms of COVID-19: a cohort study. Lancet Rheumatol 2020;2:e393–400.
[71] Otsuka R, Seino KI. Macrophage activation syndrome and COVID-19. Inflamm Regen 2020;40:19.
[72] Plassmeyer M, Alpan O, Corley MJ, Premeaux TA, Lillard K, Coatney P, et al. Caspases and therapeutic potential of caspase inhibitors in moderate–severe SARS CoV2 infection and long COVID. Allergy 2021;00:1–12.